Electrochimica Acta 168 (2015) 89–96

Contents lists available at ScienceDirect

Electrochimica Acta

journal homepage: www.elsevier.com/locate/electacta

DETERMINATION OF CURRENT MAPS BY SVET OF HOT-DIP GALVANIZED STEEL UNDER SIMULTANEOUS STRAINING

S.M. Manhabosco [a], R.J.C. Batista [b], S. Neves da Silva [a], L.F.P. Dick [a,1,*]

[a] Lab. de Processos Eletroquímicos e Corrosão, Depto. Metalurgia, Universidade Federal do Rio Grande do Sul (UFRGS), Av. Bento Gonçalves 9500, 91501.970 Porto Alegre, Brazil

[b] Depto. de Física, Universidade Federal do Ouro Preto (UFOP), Campus Morro do Cruzeiro 35400-000 Ouro Preto, Brazil

ARTICLE INFO

Article history:
Received 15 January 2015
Received in revised form 19 March 2015
Accepted 23 March 2015
Available online 25 March 2015

Keywords:
Hot-dip galvanized steel
SVET
Strain
Current map

ABSTRACT

A new experimental procedure was used to analyse the corrosion behaviour of hot-dip Zn coated steel based on the association of the scanning vibrating electrode technique (SVET) and uniaxial tensile strain applied up to 3.1% in 0.01 M NaCl solutions without release of the elastic strain during the test. The nucleation of localized corrosion sites on the coating occurs at very low strain values around the yield point and the maximum current densities increase continuously with the increase of the applied strain. The nucleation of localized corrosion on the Zn surface was favoured by the rupture of the passive film in contact with the solution by the action of slip steps and fine intergranular cracks, rather than by the exposure of the steel substrate. Straining of the Zn coating immersed in the solution was comparatively a much more aggressive condition than straining the sample in air before the corrosion tests.

© 2015 Elsevier Ltd. All rights reserved.

1. Introduction

Hot-dip zinc coatings (HD Zn) on steels have been widely used in the automotive industry, due to the excellent corrosion resistance achieved, low cost and an acceptable ductility that enables deep drawing and other cold forging processes essential to this type of industry. For this purpose, HD Zn coatings are usually applied on very ductile substrates, such as the interstitial-free (IF) steels. Good formability of the steel sheet coating is required in order to reduce cracking and to maintain the adherence of the coating to the steel substrate [1], and therefore the influence of straining on the coating adhesion is a very important parameter. The influence of straining on the corrosion of Zn-coated steels has usually been studied by the previous deformation of the coated sheet, which is only later exposed to corrosive environments [2–4]. Vagge et al. [3] observed that as deformation increases there is more delamination of the hot-dip galvanized steel sheet coating. According to Culcasi et al. [4], the harmful influence of strain on the corrosion of HD Zn coatings increases as the grain size of the coating decreases, due to the cracking of the grain boundaries of the Fe-Zn coating.

After the introduction of the scanning vibrating electrode technique (SVET) in corrosion studies by Isaacs [5–7], several authors have used this technique to study the corrosion of artificially produced, model Fe-Zn galvanic pairs [8–12] or of those produced in the cut-edge corrosion of hot-dip coatings [13–16], as well as the corrosion of Zn-electroplated samples [17,18]. Other Microelectrode techniques similar to SVET have also been used in these studies for the determination of ionic species on the corroding surface, such as scanning electrochemical microscopy (SECM) [9–10] and the scanning reference electrode technique (SRET) [19]. Microelectrode techniques were rarely associated with the straining of Zn coated sheets, and they were always performed after a previous deformation of the samples, as in the case of HD Zn coated [19], electrogalvanized [20] or electrogalvanized and additionally coated with Zn rich primer [21].

Despite the importance of zinc coatings as a corrosion protection method for steels that will suffer intense straining, there are relatively few reported studies on the influence of straining on the corrosion of Zn coated steels. These corrosion studies were always performed after straining and releasing the elastic strain before immersion of the sample in the solution [4,19–21]. The corresponding strain (ε) values by far exceeded the ones applied in this study as well as the aggressivity of the used test solutions. Culcasi et al. [4] and Berchem et al. [19] applied 10% strain to HD Zn galvanized steel before the exposure to respectively

* Corresponding author. Tel.: +55 51 33087537; fax: +55 51 33089469.
E-mail addresses: smanhabosco@gmail.com (S.M. Manhabosco), batista.rjc@iceb.ufop.br (R.J.C. Batista), sabpoa@gmail.com (S. N. da Silva), lfdick@ufrgs.br (L.F.P. Dick).
[1] ISE member.

http://dx.doi.org/10.1016/j.electacta.2015.03.162
0013-4686/© 2015 Elsevier Ltd. All rights reserved.

Table 1
Chemical composition of the interstitial free (IF) steel, wt%.

	Al	C	S	Mn	P	Ti	Nb	Si	B	N
IF Steel	0.084	0.0019	0.0093	0.257	0.028	0.003	0.008	0.008	0.0022	0.0026

0.05 M [4] and 3% NaCl [19], while Bastos et al. [20] used values of 9% and 23% before the exposure of electrogalvanized steel to 0.1 mol L^{-1} NaCl solutions. In all cases, the previous applied strain increased the corrosion, most probably due to the fracture of the coating at high ε values and exposure of the substrate before immersion in chloride solutions.

In the present work we present experimental results introducing the use of the scanning vibrating electrode technique associated with *in situ* simultaneous elastic straining of HD Zn coated steel, performed immediately after applying plastic strain to samples immersed in 0.01 M NaCl solutions.

2. Experimental

The corrosion experiments were carried out on samples cut from a 0.7 mm thick interstitial free steel (IF) sheet produced and hot-dip galvanized by *USIMINAS*, Brazil. The galvanizing was carried out by immersion in a molten Zn bath containing ~0.2 wt% Al at around 450 °C in a continuous process adjusted to a nominal coating thickness of 10 μm controlled by "N_2-knifes". The composition of the IF steel is listed in Table 1, and is characterized by a C content of only 0.0019 wt%. Microstructure and chemical composition of the Zn-based coating were determined by SEM (scanning electron microscopy) and EDS (energy dispersive X-ray spectrometry) analysis of sample cross-sections in a *5800-JEOL-NORAN* SEM. To increase the precision, EDS analysis was performed using metal standards and electron beam current measurement using a Faraday cup constituted of a grounded graphite sample provided with a 100-μm hole.

Flat specimens for uniaxial tensile tests were cut from provided steel sheets according to ASTM E8/E8M-09 [22] with dimensions as shown in Fig. 1a. A small sized (Ø = 12.3 mm, h = 5.1 mm) "*barnacle*" electrochemical cell with an electrolyte volume of 600 μL was attached to the coating surface. Good adhesion of the *barnacle* cell to the coating during the straining test was achieved using flexible cells of polypropylene and low-hardness fast cure epoxy glue. An area of approximately 1 mm^2 was exposed to the electrolyte, delimited with the use of 65 μm thick *3 M Scotch tape*. The sample was mounted on a simple device for uniaxial deformation (Fig. 1b). The *barnacle* cell was actually glued to the tape-covered surface and neither detachment of cell and tape or perceptible crevice corrosion were observed up to strain values of $\varepsilon \approx 4\%$ (0.04).

The current density map (***j***-map) acquisitions were carried out in a 0.01 mol L^{-1} NaCl solution with a measured conductivity of 1.205 mS. For this, an *Applicable Electronics Inc.* equipment controlled by the *ASET* software (*Science Wares Inc.*) was used. The vibrating microelectrode for ***j***-determinations was a Pt wire from *MicroProbes Inc.* with a spherical tip of Ø = 10 μm. To increase the sensibility of ***j***-measurements, new Pt μ-electrodes were first platinized black in a (0.1 g L^{-1} $Pb(CH_2COOH)_2 \cdot 3H_2O$ + 10 g L^{-1} $H_2PtCl_6 \cdot 6H_2O$)-solution by applying a current of −0.2 μA for 180 s and then −1.2 μA for 30 s, followed by 15 intermittent 1 s depositions with −1.2 μA. The integrity of the μ-electrode was regularly controlled in an optical microscope. When necessary, the Pt μ-electrode was recovered by repeating the second platinization step. The distance between microelectrode and sample surface was always 50 μm, and the scanned area was approximately 1 mm × 1 mm in the case of ***j***-maps, while ***j***-line scans were acquired in a length of 1 mm. Two Pt-Ir auxiliary electrodes were additionally used during the SVET measurements as a reference and for grounding, respectively. The scanning direction was always parallel to the horizontal axis of the presented SVET-maps.

The sequence of tests was the following: After delimitating the measuring window with tape and adapting the barnacle cell, samples were mounted in the straining device and exposed to the electrolyte. ***j***-line scans were immediately acquired on the unstrained samples followed by ***j***-maps measurements. Thereafter, samples were progressively plastically deformed in steps of around $\Delta\varepsilon$ = 0.8% always immersed in the test solution and ***j***-line scans were immediately measured along the direction of the applied tensile strain followed by ***j***-maps measurements without removing the applied stress. This means that ***j***-line scans and ***j***-maps were measured on samples plastically deformed immersed in the electrolyte and without relieving the elastic strain. In order to control strain values the distance between scratches or other marks was measured in the tensile deformation direction under an optical microscope. These marks were located outside the measuring window at distances within ~1 mm. The line scans consisted of 300 points with a total acquisition time of 200 s, while the ***j***-maps, respectively, of a grid of 30 × 30 points with an acquisition time of 480 s. The setting of a new strain value took between 30 and 60 s. Therefore, the progressive strain steps were applied at time intervals of around 15 min. After a total ε-value of 3.1% the experiment was interrupted and the surface cleaned for

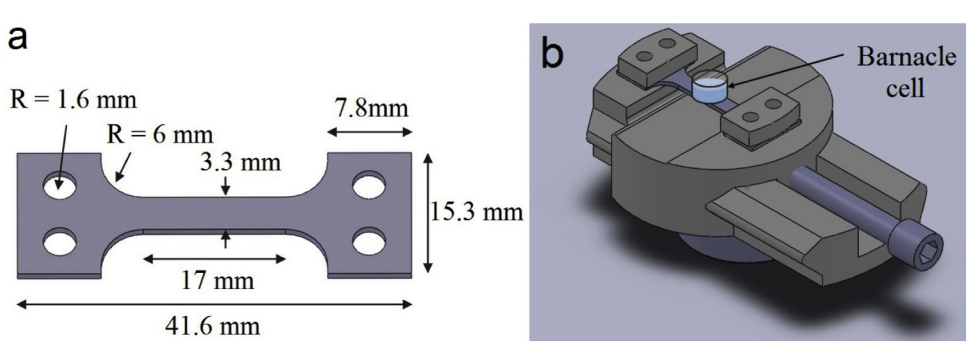

Fig. 1. a) Tensile test specimen and b) assembly of the barnacle cell on the specimen mounted in the tensile straining device.

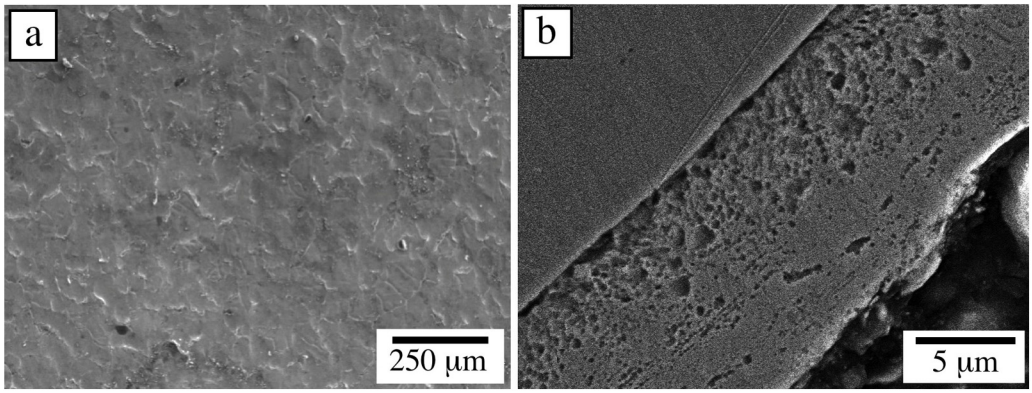

Fig. 2. SEM micrographs of hot-dip Zn coating a) top view and b) cross section.

SEM inspection of the corroded area. The same procedure was used to measure OCP transients and cyclic voltammograms (CV) after straining. Experiments were performed in triplicate.

3. Results and Discussion

The SEM micrographs of Fig. 2 show the top view of the HD Zn coating (**2a**) and its cross section (**2b**). Cross sections suffered during grinding and polishing corrosive attack due to strong galvanic coupling associated with the removal of passive layers on the Zn coating by the mechanical action. This explains the porosities of the coating, as seen on the cross section of Fig. 2b. The Zn content determined by EDS using metal standards was 93.0 wt% (87 at%) at a distance of 1.2 μm from the steel/coating interface and increased to 98.2 wt% (92.5 at%) for greater distances from the steel/coating interface, and is thus lower than expected for the composition of the outer η-phase (99.97 wt% Zn). This can be attributed to the presence of δ and ζ-phases (~$FeZn_{10}$ and ~$FeZn_{13}$) and closer to the outer surface, possibly to the occlusion of dross particles from the metal bath, increasing the measured [Fe]/[Zn] ratio. The coating had an apparent grain size around 100 μm on the surface plane (η-phase) and a mean thickness of 9.8 ± 0.3 μm.

Current density line scans measured on the surface of unstrained HD Zn samples in 0.01 mol L^{-1} NaCl show very stable values lower than 3 μA cm^2, which is in the sensibility order of the SVET method, as verified by measuring ***j*** on non conductive flat surfaces under the same conditions. The strain was then applied to the immersed samples increasing in steps progressively from ***ε*** = 0 to 0.6; 1.7; 2.2 and 3.1%. The corresponding ***j***-line scans showed very irreproducible oscillations that could only be observed immediately after straining the sample. The amplitude of ***j*** oscillations increased with the applied strain as seen for example for ε = 1.7% and ε = 3.1% in Fig. 3. The ***j*** values alternated from anodic to cathodic at distances ranging from 100 μm to 10 μm. These values are in the order or even smaller than the expected lateral resolution of SVET under the used experimental conditions, which is limited by the distance between microprobe and sample surface (≈50 μm). The time interval between two consecutive adjacent ***j*** measurement points was around one s. Thus, the observed ***j*** oscillations must be interpreted as time oscillations rather than the occurrence of stable neighbouring anodic and cathodic sites.

Possible explanations for the increase in the ***j*** oscillation between anodic and cathodic values with increasing applied ***ε*** are:

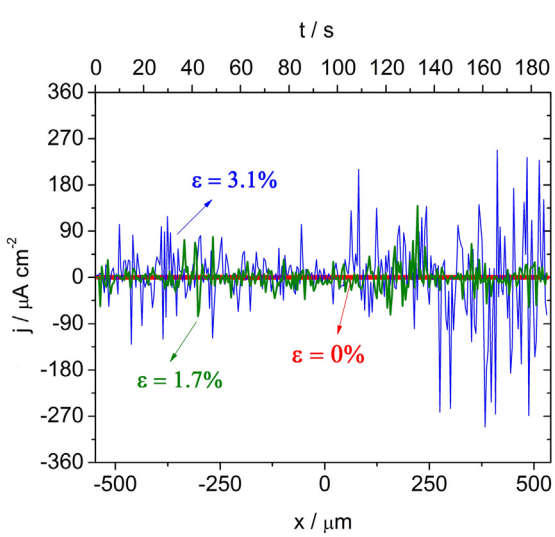

Fig. 3. Current density line scans measured on hot-dip Zn coating in 0.01 mol L^{-1} NaCl for ε values of zero, 1.7 and 3.1% (300 points).

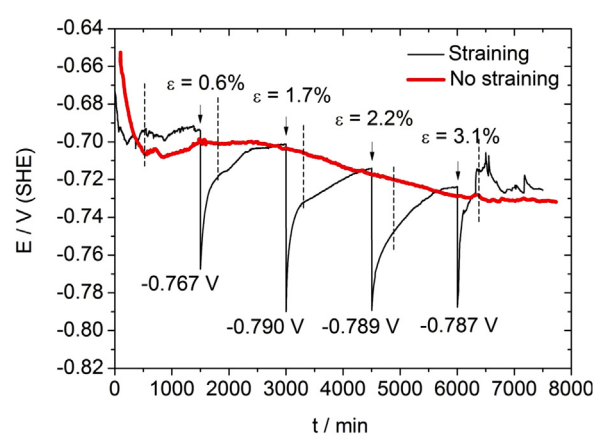

Fig. 4. OCP transients measured on progressively strained hot-dip coated samples compared to the OCP on unstrained ones in 0.01 mol L^{-1} NaCl. The arrows indicate the moment when the strain was increased and the vertical dashed lines, the beginning of a *j*-map measurement.

(a) Fracture of the whole η-Zn coating and exposure of the steel substrate, with formation of cathodic sites on the steel and anodic ones on Zn coating;
(b) Rupture of the passive film on the surface of the outer η-Zn phase due to the intersection of the slip steps with the surface, and formation of anodic sites on freshly exposed Zn surfaces and of cathodic ones on passive Zn;
(c) Cracks formed on the η-Zn surface on grain boundaries and inside grains, which stop before crossing the ζ and δ-phases forming galvanic elements between the Zn-richer and more active outer η-phase and the underlying ζ and δ-phases.

Fig. 4 shows OCP transients measured after immersion in the chloride solution of unstrained and progressively strained samples. OCP of the unstrained sample is stable up to around 2500 s at a value around −700 mV SHE, which is determined by the Zn/Zn^{2+} electrode potential ($E_{Zn^{2+}/Zn} = -762$ mV SHE + 29 mV log $[Zn^{2+}]$) and, most probably, by the potential of the oxygen reduction reaction at the partially passive Zn surface. After around 6000 s OCP drops slowly to −730 mV SHE indicating a slow activation of the surface exposed to the chloride solution. However, when the sample is strained with $\varepsilon = 0.6\%$ OCP drops rapidly to −770 mV SHE and then shifts slowly back towards the values observed for unstrained samples. For progressively higher ε values OCP drops rapidly down to values close to −790 mV SHE, shifting back to the values observed on unstrained samples within 1,000 to 1,500 s. The negative shift of OCP caused by the applied strain can be explained by the activation of the surface due to the rupture of the passive film and not by the exposure of more noble underlying phases, as Fe-richer intermetallics or even the IF steel substrate that would shift the corrosion potential towards the positive direction. Indeed, Culcasi et al. [4] observed, for HD Zn coatings 10% strained before exposing to 0.05 M NaCl, corrosion potential (E_{cor}) shifts in the negative direction up to approximately 60 mV due to slip steps formed by stretching. However, when the coating cracked during rolling, E_{cor} went to the positive direction [4,19].

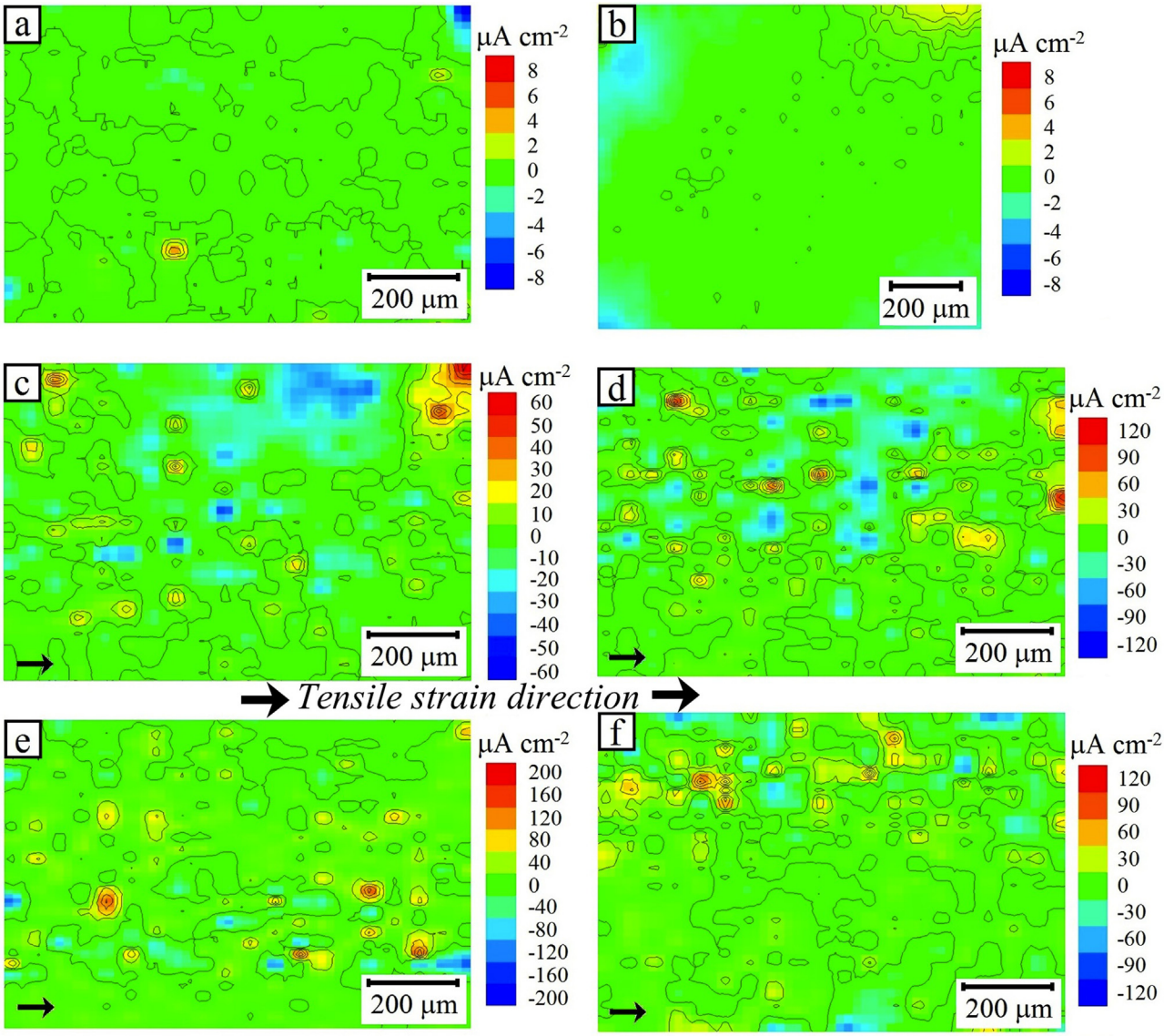

Fig. 5. Current density maps of HD Zn coated steel in 0.01 mol L^{-1}NaCl for a) $\varepsilon = 0.0\%$, and 1 min exposure, b) $\varepsilon = 0.0\%$, and 60 min exposure, c) $\varepsilon = 0.6\%$, d) $\varepsilon = 1.7\%$, e) $\varepsilon = 2.2\%$ and f) $\varepsilon = 3.1\%$. The *j* maps c), d), e) and f) were consecutively measured after *j* maps a). The black arrow indicates the direction of the applied strain.

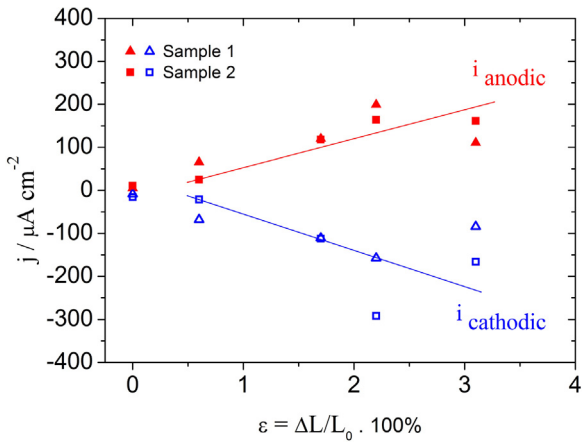

Fig. 6. Maximum anodic and cathodic current densities, j_{max}, of the hot-dip Zn coated IF steel immersed in 0.01 mol L^{-1} NaCl *versus* the applied strain ε.

After applying $\boldsymbol{\varepsilon}$ = 3.1%, detachment of the barnacle cell occurred within a certain period of time, which explains the final OCP oscillations in the experiment of Fig. 4.

It is also possible to see in Fig. 4 that the OCP-transients during their return to more positive values have apparently one or two inflection points. This indicates that the repassivation process of freshly exposed surfaces of the η-Zn is not a continuous process involving only one mechanism. One possibility is the formation of more than one Zn compound on the surface during the repassivation. Indeed, it has bee reported [23–25] that in moist atmospheres enabling electrochemical reactions amorphous-Zn $(OH)_2$ initially forms and than recrystallises to β-$Zn(OH)_2$ or dehydrates to ZnO, while in the presence of chlorides the hydroxichloride $Zn_5(OH)_8Cl_2$ is formed [26]. Moreover, on Zn electrodeposits $Zn_7(OH)_{12}Cl_2$ and ε-$Zn(OH)_2$ were found after anodic polarization in dilute Cl^- solutions [25]. The ageing of the Zn hydroxides and hydroxychlorides to ZnO to form a more stable passive film could explain the different rates of OCP variation during the return to more positive values.

After 300 s after straining and measuring the fast ***j***-line scans, OCP has suffered most of its variation due to the repassivation process (Fig. 4), allowing the measurement of more stable ***j***-maps. The time for the initiation of each ***j***-map is indicated by a vertical dashed line in Fig. 4. The corresponding ***j***-maps show that for unstrained sample (Fig. 5a), ***j*** lies initially below 8 μA cm^{-2} and after 1 h exposure to the solution even repassivation of localized corrosion sites are observed (Fig. 5b). However, for increasing $\boldsymbol{\varepsilon}$ values, localized anodic and cathodic sites can be identified (Fig. 5c–f). The maximum cathodic and anodic ***j*** *values* extracted from ***j***-maps for increasing applied strain values (Fig. 5f) are plotted in Fig. 6 for two independent measurements for which no cell detachment could be observed up to $\boldsymbol{\varepsilon} \approx 4\%$. It is possible to observe that maximum anodic and cathodic current densities $\boldsymbol{j_{max}}$ increase as the strain is increased, different to what was observed with unstrained samples exposed for the same time. Thus, the occurrence of anodic and cathodic sites in Fig. 5b–e can be attributed to the rupture of passive films on the Zn coating. The slope of $|\boldsymbol{j_{max}}|$ *versus* applied $\boldsymbol{\varepsilon}$ (Fig. 6) is roughly equal for anodic and cathodic values, $|\partial \boldsymbol{j_{max}}/\partial \boldsymbol{\varepsilon}| \approx 70$ μA cm^{-1}%$^{-1}$ and the extrapolation to ***i*** = zero lies at $\boldsymbol{\varepsilon} \approx 0.20$–0.25%. This minimum

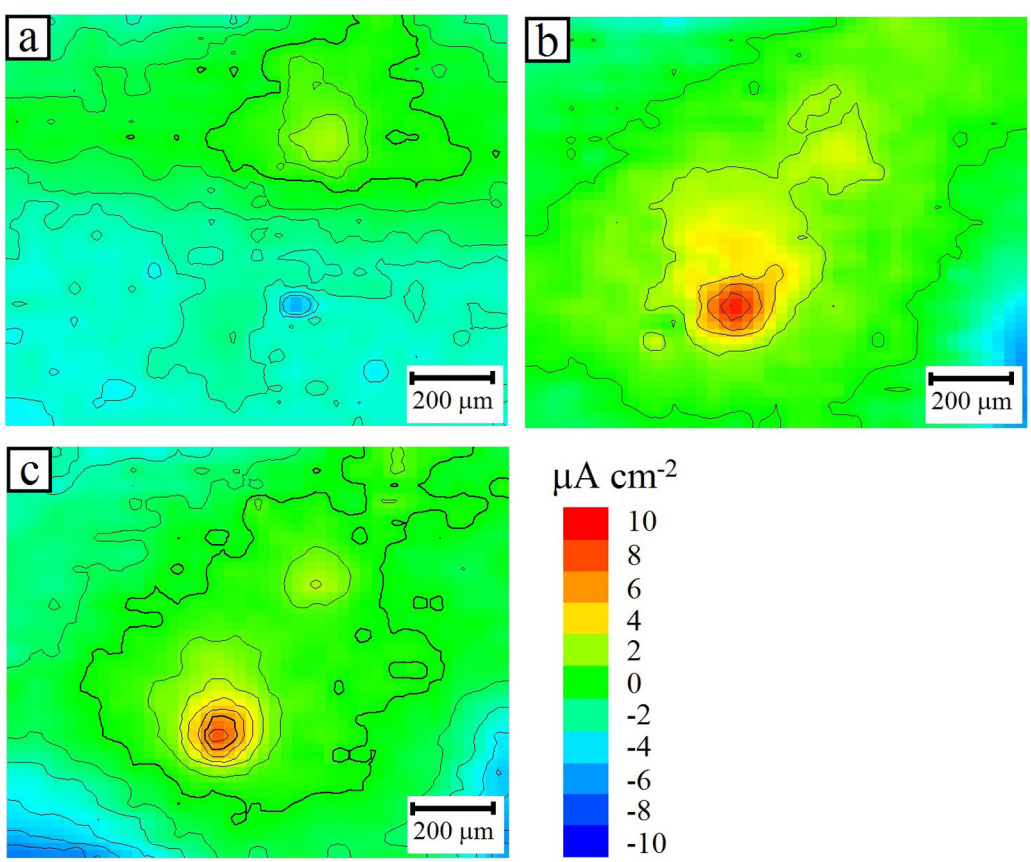

Fig. 7. Current density maps of prestrained HD Zn coated steel in 0.01 mol L^{-1} NaCl (ε = 3.1%) acquired after a) 10 s, b) 1800 s and c) 3600 s.

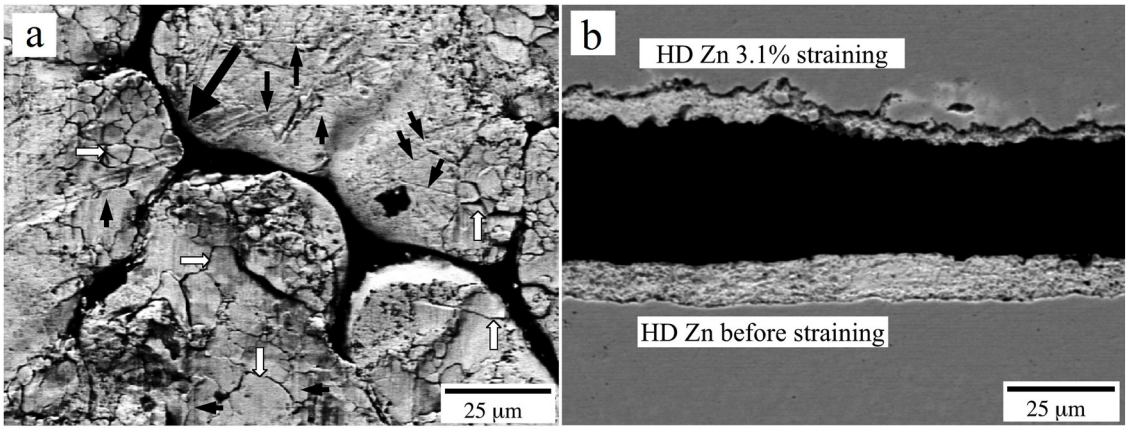

Fig. 8. SEM micrographs of hot-dip Zn coating after 3.1% straining in 0.01 mol L^{-1} NaCl: a) Top view and b) cross section. Small black arrows indicate slip steps, large black arrow indicates grain boundary crack, and small white arrows indicate transgranular cracks.

strain value is possibly related to the elastic strain limit of the sample, at which slip steps begin to form on the coating surface.

It should be observed that samples deformed up to $\varepsilon = 3.1\%$ in air a day before immersion in the 0.01 mol L^{-1} NaCl solution show after exposure $\boldsymbol{j}$ values lower than 10 μA cm^{-2}, as shown in Fig. 7 after a) 10, b) 1800 and c) 3600 s exposure in the chloride solution. The maximum $\boldsymbol{j}$ values for "dry" pre-strained samples (Fig. 7) are slightly higher than for unstrained samples, however well below the values observed when ε was applied to the immersed sample and the $\boldsymbol{j}$-map measured without releasing the elastic strain. Additionally, the density of localized corrosion sites is much higher, when ε is applied to the immersed sample. This shows that corrosion tests with pre-strained samples are less aggressive than *in situ* straining due to the increased nucleation of localized corrosion when slip steps fracture the passive film in contact with the chloride solution.

An inspection of the HD Zn coating after the experiments up to $\varepsilon = 3.1\%$ (Fig. 8a, b) reveals that the steel/coating interface roughness increased during the corrosion + deformation experiment, indicating that coating and substrate were plastically deformed, as seen in the cross sections of Fig. 8a comparing the interfaces before (Fig. 8a, bottom) and after experiments (Fig. 8a, top). This is in accordance with ε values applied above the yield point. Although the upper part of the coating was damaged by preparation of the cross sections, it can be seen from Fig 8a that cracks do not cross the whole coating down to the substrate. Hence, the observed cathodic sites are not associated with exposed steel surfaces.

The top view of the sample shows an apparent attack of grain boundaries (big black arrows in Fig. 8b), which is compatible with the medium grain size of the outer η-Zn phase in the order of 100 μm (Fig. 2a). The cracking of grain boundaries of previously strained HD Zn coatings and their corrosion attack after exposure were observed before [4]. However, several smaller cracks inside the 100 μm-grains are also visible separated by mean distances ranging from 5 to 10 μm (small black arrows in Fig. 8b). In addition, slip steps are visible on the top of the coating after the experiments (white arrows in Fig. 8b). These finer defects may be associated with the initial $\boldsymbol{j}$ oscillations between anodic and cathodic values observed in the non-stationary $\boldsymbol{j}$-line scans (Fig. 3).

To verify the influence of plastic and elastic strains on the localized corrosion of the Zn coating, CV curves with 20 mV s^{-1} were additionally acquired in 0.01 M NaCl for different straining conditions (Fig. 9). Very low current densities are observed for unstrained samples in the potential range between −970 and −480 mV SHE (Fig. 9, label *w/o def*), showing that the η-Zn surface remains passive in this E interval.

However, if the sample is strained up to $\varepsilon = 3.1\%$ under dry conditions and CV acquired 24 h later, $\boldsymbol{j}$ starts increasing at $\boldsymbol{E} \approx -650$ mV SHE and, at the beginning of the reverse scan, continues growing (Fig. 9, label *dry* (*pl*) *def*), as expected for the onset of pitting corrosion. Under these conditions, pit repassivation is observed at $E \approx -725$ mV SHE (Fig. 9, label *dry* (*pl*) *def*). If the elastic strain is not released after applying the plastic strain, as seen in Fig. 8 in the curve labelled "*dry* (*pl + el*) *def*)", the pitting potential shifts slightly in the negative direction, without significant variation of the repassivation potential. Even though, the anodic charge flowed during pitting approximately doubles. Thus, elastic ε promotes the further growth of the active dissolution front without interfering much on nucleation and repassivation phenomena.

A complete different behaviour is observed when the sample is strained while immersed in the chloride solution and CV is measured a few seconds after straining the sample without releasing the elastic strain (Fig. 9, label *wet* (*pl*) *def*). In this case, the

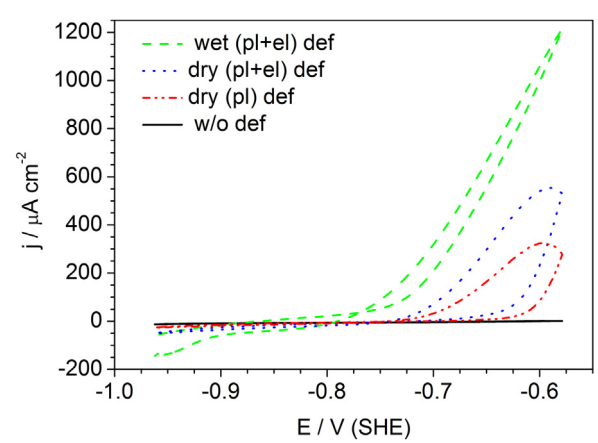

Fig. 9. Cyclic voltammetric curves (0.01 mol L^{-1} NaCl, 20 mV s^{-1}) of hot-dip Zn coating under different conditions. Undeformed: *w/o def*. Strained previously in air: *dry* (*pl*) *def*). Strained in air without releasing the elastic strain: *dry* (*pl + el*) *def*. Strained in the solution a few seconds before CV acquisition: *dry* (*pl + el*) *def*.

current rise is observed at a potential close to the standard equilibrium potential of Zn^{2+}/Zn, at $E \approx -775$ mV SHE without showing a passive current plateau, and ***j*** approaches zero as this potential is achieved again during the reverse scan. The ***j*** hysteresis, typical of localized corrosion, is no longer observed, because of the change of the corrosion mechanism from pitting of the passive η-Zn surface to its uniform corrosion. It is noteworthy that cathodic currents also slightly increase with the applied strain, indicating that the passive layer formed on the η-Zn phase under dry conditions was disrupted and not completely restored for a certain time. The observed cathodic ***j***-increase is in accordance with the occurrence of localized cathodic sites, as observed on the ***j*** maps of SVET (Fig. 5) when strain is applied.

It can be concluded that a slip dissolution phenomenon of η-Zn of the coating occurs at low strain values, promoting the nucleation of pits and lowering the pitting potential. The "slip dissolution model" has been proposed in the 60's [e.g. [27]] and intensively studied in the 80's as a mechanism of stress corrosion cracking (SCC) of stainless steels [28,29] and Al-alloys [30–32]. The strain influence on SCC of those alloys was experimentally verified by observing the nucleation of cracks on slip steps, which form at the intercept of persistent slip bands (PSB) with the metal surface [27]. Additional evidence was found by observing microtunnels at slip steps, united by crack propagation [33]. According to this SCC mechanism, an increment of crack length will lead to the formation of PSB at the new position of the crack tip and to new microtunnels in a continuing process of crack growth of the stressed material. In this work, the influence of slip step dissolution on the corrosion of the Zn coating was directly verified by measuring the current density by CV and SVET experiments at very low strain values. More recently, Zhu *et al.* [34] observed pit nucleation and SCC of austenitic stainless steel submitted to low elastic strain similar to the values used in this work.

If the CV is measured just after straining the immersed sample, the surface repassivation is not complete, enabling a higher degree of active dissolution of the Zn surface by uniform corrosion besides the increase of cathodic currents. As verified in the OCP transients of Fig. 4, around 400 s after straining and exposure of the surface to the chloride solution, the passive film is reconstructed and localized corrosion will again be the major corrosion mechanism, however maintaining the influence of previous applied plastic strain. The elastic strain help will help the disruption of the passive film enhancing uniform and localized corrosion.

4. Conclusions

The corrosion of HD Zn coated steel strained in contact with 0.01 M NaCl solution without release of the elastic strain is much more intense compared to unstrained samples exposed during the same time, or to samples previously strained in air and than exposed to the solution during the same time.

In the case of straining the immersed surface, the corrosion mechanism changes from localized to uniform corrosion, specially if the polarization is applied within a fez seconds after straining. After repassivation of the surface, the influence of previous straining is still verified by a lower pitting potential and higher anodic current densities. This is explained by slip dissolution that helps the nucleation of pits on the passive surface or to the disruption of the passive layer promoting uniform corrosion.

Maximum anodic and cathodic current densities increase at approximately the same rate as the applied strain is continuously increased with a value of roughly 70 $\mu A\,cm^{-2}$ per percentage strain increment.

The nucleation of localized corrosion sites occurs at ultra low strain values around the yield point or even lower. The nucleation is favoured by the rupture of the passive film on the Zn surface by the action of slip steps and fine intergranular cracks in contact with the solution, rather than due to the fracture of the coating and exposure of the steel substrate.

Acknowledgments

The authors acknowledge the financial support of *USIMINAS* and *CAPES*, and the *Centro de Microscopia Eletrônica* of *UFRGS* for the use of facilities.

References

[1] A.K. Gupta, D.R. Kumar, Formability of galvanized interstitial-free steel sheets, Journal Materials Processing Technology 172 (2006) 225.
[2] E.A. Sacco, N.B. Alvarez, J.D. Culcasi, C.I. Elsner, A.R. Di Sarli, Effect of the plastic deformation on the electrochemical behavior of metal coated steel sheets, Surface & Coatings Technology 168 (2003) 115.
[3] S.T. Vagge, V.S. Raja, R.G. Narayanan, Effect of deformation on the electrochemical behavior of hot-dip galvanized steel sheets, Applied Surface Science 253 (2007) 8415.
[4] J.D. Culcasi, C.I. Elsner, A.R. Di Sarli, Effect of zinc crystals size on galvanized steel deformation and electrochemical behaviour, Materials Research 12 (2009) 273.
[5] H.S. Isaacs, Y. Ishikawa, Applications of the vibrating probe to localized current measurements, Proceedings NACE Corrosion/85, March 25–29, Paper 55 (1985).
[6] H.S. Isaacs, Initiation of stress corrosion cracking of sensitized type 304 stainless steel in dilute thiosulfate solution, Journal Electrochemical Society 135 (1988) 2180.
[7] H.S. Isaacs, The measurement of the galvanic corrosion of soldered copper using the scanning vibrating electrode technique, Corrosion Science 28 (1988) 547.
[8] R.M. Souto, Y. Gonzalez-Garcıa, A.C. Bastos, A.M. Simões, Investigating corrosion processes in the micrometric range: A SVET study of the galvanic corrosion of zinc coupled with iron, Corrosion Science 49 (2007) 4568.
[9] A.M. Simões, A.C. Bastos, M.G. Ferreira, Y. Gonzalez-Garcıa, S. Gonzalez, R.M. Souto, Use of SVET and SECM to study the galvanic corrosion of an iron–zinc cell, Corrosion Science 49 (2007) 726.
[10] J. Izquierdo, L. Nagy, S. González, J.J. Santana, G. Nagy, R.M. Souto, Resolution of the apparent experimental discrepancies observed between SVET and SECM for the characterization of galvanic corrosion reactions, Electrochemistry Communications 27 (2013) 50.
[11] S. Kallip, A.C. Bastos, M.L. Zheludkevich, M.G.S. Ferreira, A multi-electrode cell for high-throughput SVET screening of corrosion inhibitors, Corrosion Science 52 (2010) 3146.
[12] S. Kallip, A.C. Bastos, K.A. Yasakau, M.L. Zheludkevich, M.G.S. Ferreira, Synergistic corrosion inhibition on galvanically coupled metallic materials, Electrochemistry Communications 20 (2012) 101.
[13] M. Challis, D.A. Worsley, Cut edge corrosion mechanisms in organically coated zinc–aluminium alloy galvanised steels, British Corrosion Journal 36 (2001) 297.
[14] I.M. Zin, S.B. Lyon, A. Hussain, Under-film corrosion of epoxy-coated galvanised steel An EIS and SVET study of the effect of inhibition at defects, Progress in Organic Coatings 52 (2005) 126.
[15] D.J. Penney, J.H. Sullivan, D.A. Worsley, Investigation into the effects of metallic coating thickness on the corrosion properties of Zn–Al alloy galvanising coatings, Corrosion Science 49 (2007) 1321.
[16] F. Thébault, B. Vuillemin, R. Oltra, K. Ogle, C. Allely, Investigation of self-healing mechanism on galvanized steels cut edges by coupling SVET and numerical modeling, Electrochimica Acta 53 (2008) 5226.
[17] A.C. Bastos, A.M. Simões, M.G. Ferreira, Corrosion of electrogalvanized steel in 0.1M NaCl studied by SVET, Portugaliae Electrochimica Acta 21 (2003) 371.
[18] A.M. Simões, J.C.S. Fernandes, Studying phosphate corrosion inhibition at the cut edge of coil coated galvanized steel using the SVET and EIS, Progress in Organic Coatings 69 (2010) 219.
[19] K. Berchem, M.G. Hocking, The influence of pre-straining on the corrosion fatigue performance of two hot-dip galvanised steels, Corrosion science 48 (2006) 4094.
[20] A.C. Bastos, M.G.S. Ferreira, A.M.P. Simões, Effects of mechanical forming on the corrosion of electrogalvanised steel, Corrosion Science 69 (2013) 87.
[21] A.G. Marques, A.M. Simões, EIS and SVET assessment of corrosion resistance of thin Zn-55% Al-rich primers: Effect of immersion and of controlled deformation, Electrochimica Acta 148 (2014) 153.
[22] EASTM E8/E8M-13a, Standard Test Methods for Tension Testing of Metallic Materials, ASTM, International, West Conshohocken, PA, 2013.
[23] M. Ueda, M. Matsuda, T. Ohtsuka, Atmospheric Corrosion of Zinc and Zinc Alloys Using In-Situ Raman Spectroscopy, The Electrochemical Society 14 (2004) 166–172.

[24] T.E. Graedel, Corrosion Mechanisms for Zinc Exposed to the Atmosphere, Journal of The Electrochemical Society 136 (1989) 193–203.
[25] M.C. Bernard, A. Hugot-Le Goff, N. Phillips, In Situ Raman Study of the Corrosion of Zinc-Coated Steel in the Presence of Chloride, Journal of The Electrochemical Society 142 (1995) 2167–2170.
[26] W. Miao, I.S. Cole, A.K. Neufeld, S. Furman, Pitting Corrosion of Zn and Zn-Al Coated Steels in pH 2 to 12 NaCl Solutions, Journal of The Electrochemical Society 154 (2007) C7–C15.
[27] P.R. Swann, H.W. Pickering, Implications of the Stress Aging Yield Phenomenon with Regard to Stress Corrosion Cracking, Corrosion NACE 19 (1963) 369t–372t.
[28] T. Nakayama, M. Takano, Application of a Slip Dissolution-Repassivation Model for Stress Corrosion Cracking of AISI 304 Stainless Steel in a Boiling 42% $MgCl_2$ Solution, Corrosion 42 (1986) 10–15.
[29] P.L. Andresen, Environmentally Assisted Growth Rate Response of Nonsensitized AISI 316 Grade Stainless Steels in High Temperature Water, Corrosion 44 (1988) 450–460.
[30] F.P. Ford, Quantitative examination of slip-dissolution and hydrogen-embrittlement theories of cracking in Al alloys, Materiasls Science and Technology 12 (1978) 326–334.
[31] M.P. Mueller, A.W. Thompson, I.M. Bernstein, Stress Corrosion Behavior of 7075 Aluminum in 1N Aluminum Chloride Solutions, Corrosion 41 (1985) 127–136.
[32] K.R. Cooper, R.G. Kelly, Measurement and Modelling of Crack Conditions during the environment-assisted cracking of Al-Zn-Mg-Cu Alloy, TMS Annual Meeting, Proc. of Symp. on Chemistry and Electrochemistry of Corrosion and Stress Corrosion, Warrendale, PA, 2001.
[33] P.R. Swann, J.D. Embury, in: V.F. Zackay (Ed.), High Strength Materials, John Wiley, 1965, pp. 327–362.
[34] L.K. Zhu, Y. Yan, L.J. Qiao, A.A. Volinsky, Stainless Steel Pitting and Early-stage Stress Corrosion Cracking Under Ultra-low Elastic Load, Corrosion Science 77 (2013) 360–368.